

Article

Gold Migration and Precipitation as Collaurum in Orogenic Gold Deposits: Constrains from Microscopic Gold Particles Observed in the Alteration Zone in Shangong Gold Ore, Henan, China

Yu Qiao ^{1,2}, Zhixuan Han ^{3,4,*}, Bimin Zhang ¹, Xiaocheng Wei ⁴, Chunfang Dong ⁴ and Hanliang Liu ^{1,*}

¹ Institute of Geophysical and Geochemical Exploration, Chinese Academy of Geological Sciences, Langfang 065000, China; qiaoyucugb@163.com (Y.Q.); zbimin@hotmail.com (B.Z.)

² Zijin Mining Group Co., Ltd., Longyan 364200, China

³ Institute of Mineral Resources, Chinese Academy of Geological Sciences, Beijing 100037, China

⁴ Collaborative Innovation Center for Exploration of Nonferrous Metal Deposits and Efficient Utilization of Resources by the Province and Ministry, Guilin University of Technology, Guilin 541004, China; wx08241999@163.com (X.W.); 15132401513@163.com (C.D.)

* Correspondence: hanzhixuan@glut.edu.cn (Z.H.); liuhanliang912@163.com (H.L.)

Abstract: Aqueous complexation has long been considered the only viable means of transporting gold to depositional sites in hydrothermal ore-forming systems. Here, we present direct evidence supporting an alternative hypothesis, namely, the transport of gold as colloidal particles. We observed nano-scale gold particles adsorbed on halloysite and micro-scale gold particles in altered rocks by TEM and SEM in the Shangong orogenic gold deposit. Based on this evidence, we propose a feasible model for the origin of microscopic gold particles in alteration zones. In the early stage of ore-forming fluid, gold may migrate in the form of collaurum, which is maintained by supercritical CO₂ and colloidal silica. Low salinity and high pressure are conducive to the stable migration of colloidal gold. When the physicochemical conditions change, some collaurum is precipitated and adsorbed by the clay minerals produced by hydrothermal alteration, and some collaurum undergoes growth and evolves into micro-submicrometer-sized gold particles. This study highlighted the significance of collaurum in the formation of orogenic gold deposits.

Keywords: colloidal gold; nanoparticles; clay minerals; carbon dioxide; Shangong gold deposit



Citation: Qiao, Y.; Han, Z.; Zhang, B.; Wei, X.; Dong, C.; Liu, H. Gold Migration and Precipitation as Collaurum in Orogenic Gold Deposits: Constrains from Microscopic Gold Particles Observed in the Alteration Zone in Shangong Gold Ore, Henan, China. *Minerals* **2024**, *14*, 327. <https://doi.org/10.3390/min14030327>

Academic Editor: Vratislav Hurai

Received: 23 February 2024

Revised: 19 March 2024

Accepted: 20 March 2024

Published: 21 March 2024



Copyright: © 2024 by the authors. Licensee MDPI, Basel, Switzerland. This article is an open access article distributed under the terms and conditions of the Creative Commons Attribution (CC BY) license (<https://creativecommons.org/licenses/by/4.0/>).

1. Introduction

The mechanism of activation, migration, and precipitation of elements is the basic research concept in the formation of metal deposits [1]. Clarifying the existence of gold (Au) in the process of mineralization is crucial to understanding how gold deposits form. Previous studies have suggested that the transportation of Au in ore-forming fluids depends on sulfide complexes and chloride complexes [2–5]. Gold sulfide and hydrogen sulfide species (e.g., Au(HS)₂[−] and Au(HS)⁰) are believed to be more efficient for transporting gold [6]. In particular, recent research suggests that the trisulfur radical ion S^{3−}, which can exist stably in aqueous fluid under a wide range of temperatures (from 200 °C to 700 °C) and pressure conditions (from saturated vapor pressure to 30 kbar), may play an important role in gold transport [7–10].

There has long been a huge controversy as to whether gold can be transported stably in the form of collaurum in hydrothermal ore-forming systems. Direct observation of gold nanoparticles in a Carlin-type gold ore-forming system confirmed that nano-gold is a key link in the metallogenic process [11]. This raises the question of whether the gold nanoparticles observed in the ore rocks are just the result of the precipitation of

gold complexes or whether the gold directly migrated as colloidal particles in the ore-forming fluid. In fact, the well-developed colloform textures in the mineral scales in hydrothermal gold deposits are considered strong evidence that gold can be transported as colloids [12–14]. Advancements in technology and experimental petrology have enabled the observation of gold nanoparticles in simulation experiments and natural fluids and media [15–17]. Submicron/nano gold particles were found in high-temperature volcanic gas deposits [18,19], and nanoscale hexagonal crystals of Cu and Au alloy were observed in earthgas and soil collected at the Jinwozi goldfield [20]. More recently, gold nanoparticles in the fluid of the Reykjavik geothermal field in Iceland [21] and gold colloids in black smoker hydrothermal fluids ejected from the submarine hydrothermal vents of the South Pacific [22] were detected, confirming that gold nanoparticles can exist and migrate stably in the hydrothermal fluid. All these demonstrate that gold (bio) colloids could be an important component of gold dispersion in the environment [23].

Orogenic gold deposits, which supply ~30% of gold resources worldwide, were formed by massive aqueous–carbonic fluid flow along major fault zones during orogeny, typically during late orogenic shifts from compressional to transpressional or transtensional regimes [24,25]. Despite decades of study, the genesis of orogenic gold deposits remains a topic of debate [26,27]. One aspect of this debate concerns the state of gold in mineralizing fluids, specifically whether nano-gold can play a role in the mineralization process. Some research has found evidence for the existence of collaurum in orogenic gold deposits. Gold nanoparticles were observed in the CO₂-rich gas-liquid inclusions in the gold-rich layer of the Russian Kola Super-Deep Borehole by LA-ICP-MS and optical methods, and these fluids were interpreted as a precursor of ore-forming fluids for orogenic gold deposits [28]. Submicron gold particles on the inner walls or on calcite or baryte crystals of open inclusions of orogenic gold ore were observed by scanning electron microscopy (SEM) and might be formed by the growth of gold nanoparticles present in the ore-forming fluid [29]. More direct evidence for the transport of the gold as colloidal particles and their flocculation in nanoscale calcite veinlets was presented by McLeish et al. [30].

The Shangong gold deposit is a typical orogenic gold deposit that is characterized by reduced salinity, CO₂-rich ore fluids, and fault-controlled ore bodies [31–33]. Structure-altered zones are a typical feature of orogenic gold deposits [34,35]. If gold nanoparticles exist in the ore-forming fluid, they will leave traces when the ore-forming fluid interacts with the wall rocks. In our previous work, micro-submicrometer-sized gold particles in ore rocks have been found [36]. Here, we further present the gold nanoparticles observed in the alteration zone and discuss the migration and precipitation of gold as colloidal gold.

2. Geological Background

The Shangong gold deposit is located in the Xiong'er Terrane, Henan Province, on the southern margin of the North China Craton, and is bounded by the San–Bao fault to the north and the Machaoying fault to the south [37] (Figure 1). The NE-trending faults are the most developed in the study area, and the Shangong gold deposit is controlled by the Kangshan–Qiliping fault (KQF in Figure 1C). The whole ore belt is like a broom, which gradually spreads out from southwest to northeast (Figure 2). The accumulated gold resources of the Shangong gold deposit reach 105 tons. The ore types are mainly structural breccia type, structural mud conglomerate type, and altered rock type. The major ores of this deposit have a disseminated, vein-disseminated, and breccie-like structure. The ore bodies are mainly pod-like, vein-like, and lenticular. The main metallic minerals are pyrite, followed by galena, sphalerite, chalcopyrite, fahlore, and pyrrhotite. The gangue minerals are mainly quartz, ankerite, and sericite, followed by chlorite, fluorite, and a small amount of barite and calcite. The wall rocks of the mining area is intensively altered, and the main alteration minerals are quartz, ankerite, sericite, chlorite, hematite, followed by kaolinite, fluorite, and a small amount of barite. From the orebody outward to the wall rocks, the alteration sequences and their corresponding homogenization temperatures of fluid inclusions are: Au-bearing sulfide-ankerite-sericite-quartz zone (320 °C~390 °C)→sericite-

chlorite zone (230 °C~300 °C)→sericite-ankerite zone (180 °C~240 °C)→ankerite-hematite zone (110 °C~200 °C) [32,33].

The origin of ore-forming materials and ore-forming fluids in the Shanggong gold deposit has been debated by different researchers [31,37–39]. According to previous studies, the mineralization of the Shanggong gold deposit can be divided into three stages. In the first stage, the Taihua complex experienced two stages of tectonic metamorphism in Archean [40], and part of gold could be locally enriched in the favorable tectonic fracture dilatation zone to form an “ore embryo” [32]. The second stage is mainly Indosinian mineralization [41,42], consistent with the continental collision of the North China Plate and the Yangtze Plate, in which metamorphic fluid generated by the collision orogeny further extracted gold from the Taihua Group complex and “ore embryo”. The third stage is Yanshanian mineralization, the main mineralization stage, which is consistent with the large-scale gold mineralization in the Xiongershan area [43]. This period is mainly due to the transition of the tectonic environment from compression to extension, which is directly related to the thinning of the lithosphere in the North China Craton and the remelting of the crystalline basement of the lower crust [40,44,45]. The geological characteristics of the Shanggong gold deposit are basically consistent with the Mesozoic collision orogeny in the southern margin of the North China Craton, and the mineralization is not only related to the metamorphic fluid generated by the continental collision orogeny but also controlled by the Yanshanian magmatic hydrothermal fluid [46,47]. So both the mantle and the Taihua complex contributed partial metallogenic materials of the Shanggong gold deposit [39].

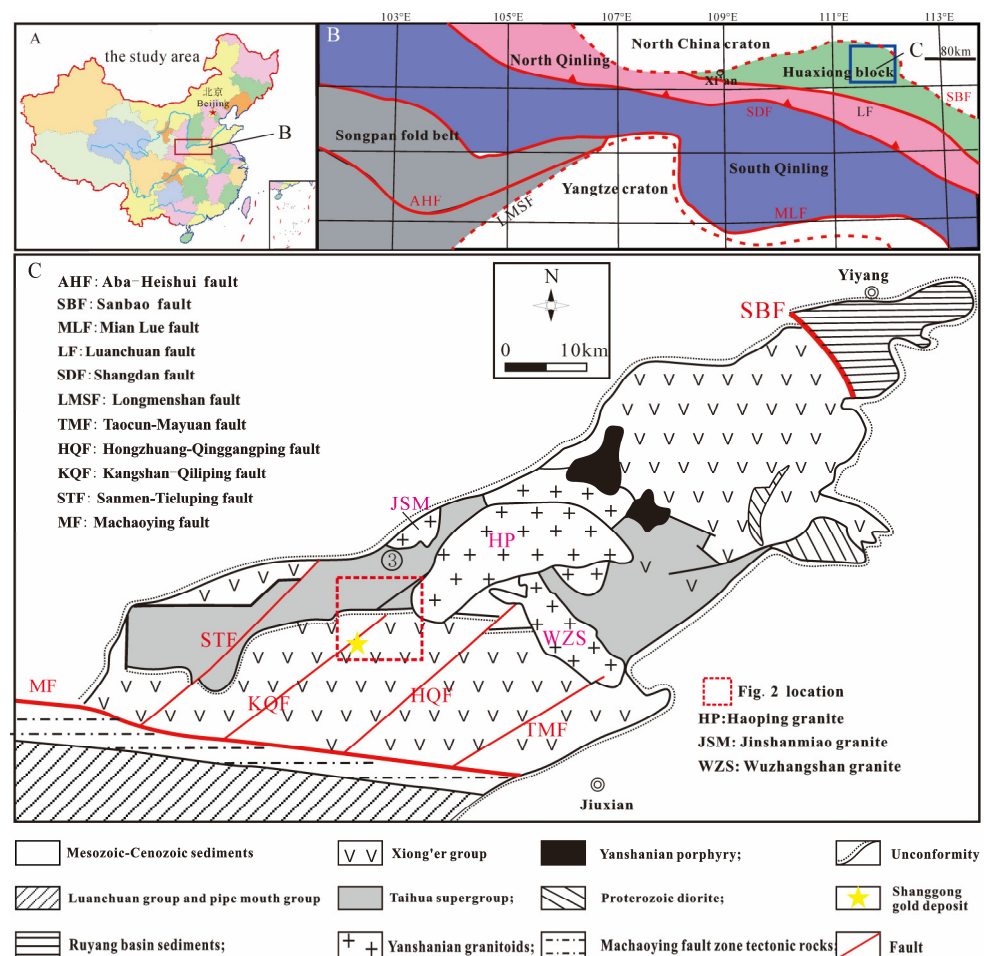


Figure 1. (A) geographical location of the study area; (B) tectonic location of the study area; (C) simplified geological map of the Xiong'er Terrane showing the location of the Shanggong Au deposit (modified after [48]).

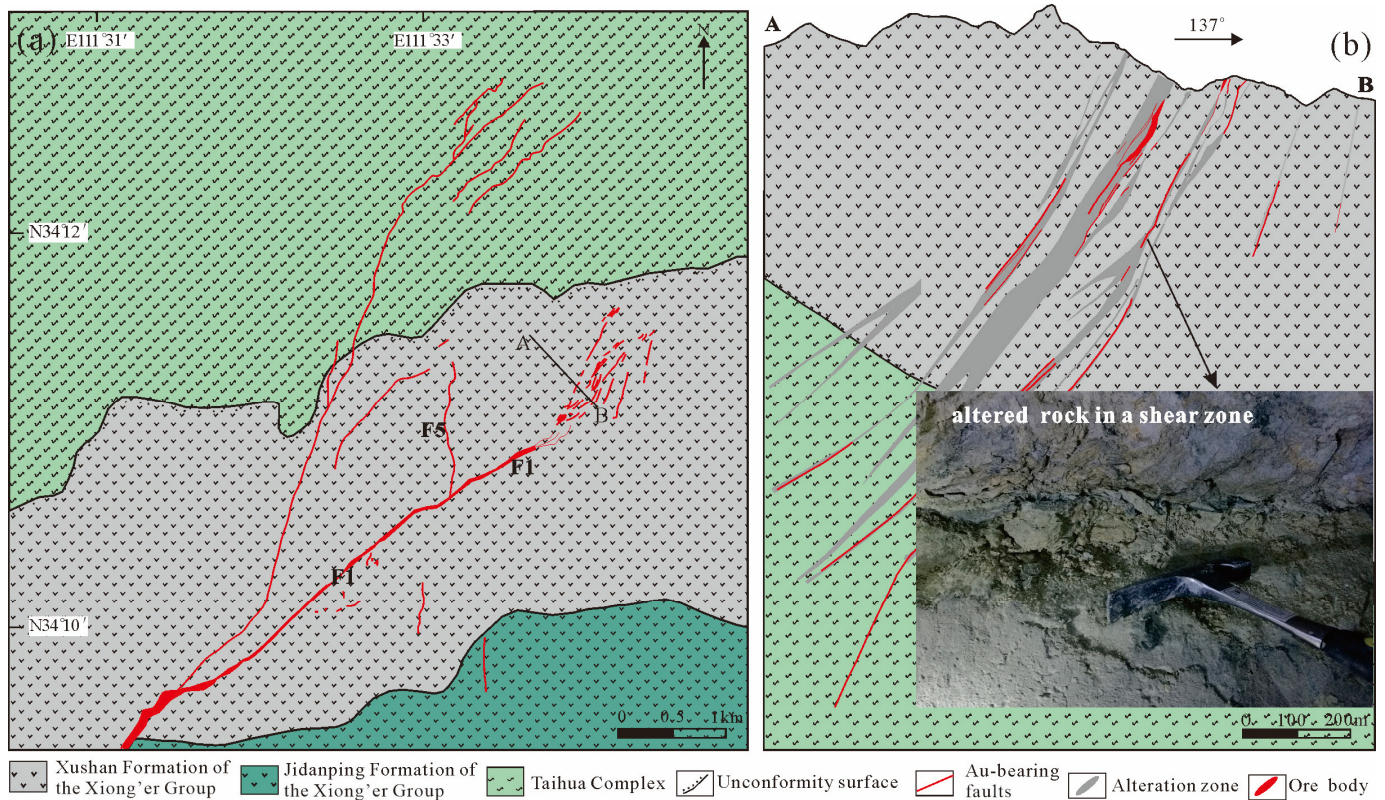


Figure 2. (a) Simplified geological map of the Shanggong gold deposit. (b) The geological map of the 33rd exploration profile and the field picture of the altered rock (modified after [38]).

3. Sampling and Analysis Methods

3.1. Sample Collection and Preparation

The altered rock sample (chlorite alteration zone) was collected from the mining roadway in the 33rd exploration line (Figure 2). It was dried at room temperature and ground to <75 μm for chemical analysis. The uncrushed sample was randomly dispersed onto the conductive glue for SEM observation. The nanoparticles of the altered rock were collected with independently designed equipment, which is composed of an electromagnetic oscillator, a micron sieve, a capture device, and a vacuum pump (Figure 3). During the scattering process, the nanoparticles of the altered rocks with the rising gases entered the capture device through a 0.45-μm Millipore filter and were captured on the copper (Cu) grids.

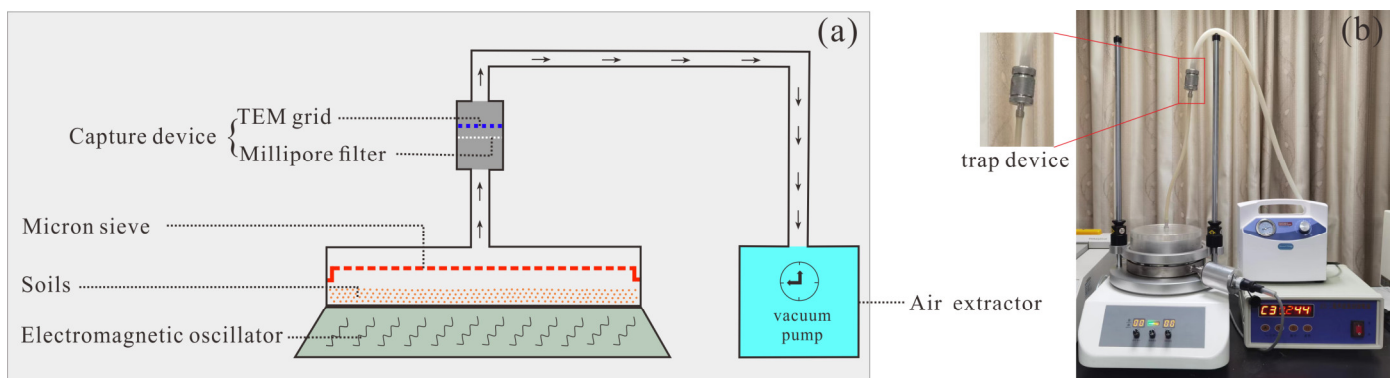


Figure 3. The equipment used for collecting nanoparticles from the altered rock samples: (a) model diagram; (b) physical device.

3.2. Analytical Methods

3.2.1. TEM Analysis

The TEM observations of particles were conducted using a Thermo Scientific (Waltham, MA, USA) FEI Talos F200S microscope operated at 200 kV at the Electron Microscopy Center of GIGCAS (Guangzhou Institute of Geochemistry, Chinese Academy of Sciences, Guangzhou, China). Various techniques, including scanning TEM (STEM), high-resolution TEM (HRTEM), selected area electron diffraction (SAED), and energy dispersive spectroscopy (EDS), were used for morphological, structural, and compositional investigations.

3.2.2. SEM Analysis

Scanning electron microscopy (SEM) with EDS was utilized to study the surface microtopography and chemical composition of the altered rock samples. For more detailed information on SEM, see Han et al. [36]. SEM observation of the altered rock sample was conducted at Guilin University of Technology (GLUT).

3.2.3. Chemical Analysis

The altered rock was ground to <75 μm and sent to the central laboratory of the Institute of Geophysical and Geochemical Exploration, China Geological Survey. The major elements (SiO_2 , Al_2O_3 , TFe_2O_3 , MgO , CaO , K_2O , S) were analyzed with X-ray Fluorescence Spectroscopy (XRF). The concentration analysis of Na_2O and Au was conducted with an Inductively Coupled Plasma Optical Emission Spectrometer (ICP-OES) and a Graphite Furnace Atomic Absorption Spectrometry (GF-AAS). The passing rates of standard reference material and laboratory duplicate samples were both 100% for SiO_2 , Al_2O_3 , TFe_2O_3 , MgO , CaO , K_2O , Na_2O , and S. The passing rate of the laboratory duplicate samples for Au was 90.9%. To assess the chemical weathering degree of the rocks, the chemical index of alteration (CIA) was calculated based on the formula $\{x(\text{Al}_2\text{O}_3)/[x(\text{Al}_2\text{O}_3) + x(\text{CaO}) + x(\text{Na}_2\text{O}) + x(\text{K}_2\text{O})]\} \times 100$, where the oxides are in molecular percentage.

4. Results

4.1. Chemical Composition

The chemical composition of the altered rock is listed in Table 1. The ore rock and altered rock were both mainly composed of Si, Al, Fe, Ca, K, Mg, and O. The Au concentration is 877 ng/g. The S concentration is not high, indicating the sulfides are not enriched in the alteration zone. The CIA value of the altered rock (57.99) is very low, which suggests that the alteration zone is not subjected to intense chemical weathering.

Table 1. Chemical compositions and CIA of the altered rock (SGAR) of the Shanggong gold deposit.

Elements	S	Au	SiO_2	Al_2O_3	TFe_2O_3	MgO	CaO	Na_2O	K_2O	CIA
Unit	$\mu\text{g/g}$	ng/g	%	%	%	%	%	%	%	
SGAR	113	877	58.3	17.2	6.01	1.88	3.65	0.98	3.88	57.99

4.2. SEM Observation of the Altered Rock

Under SEM observation, the altered rocks are mainly composed of clay minerals. Most of the clay minerals are chlorite and kaolinite. A small amount of pyrite, barite, galena, and ankerite exist in the altered rock sample. The native gold particles are also found, which are not bound with clay minerals and pyrites. Considering that pyrites tend to be oxidized to iron (hydro)oxides in the epigenetic process, it is important to point out that the pyrites in the altered rock are all regular-shaped (see Figure 4B,C) and no iron oxides and hydroxides were observed, which certifies that the clay minerals and native gold particles are very likely formed during the ore-forming process.

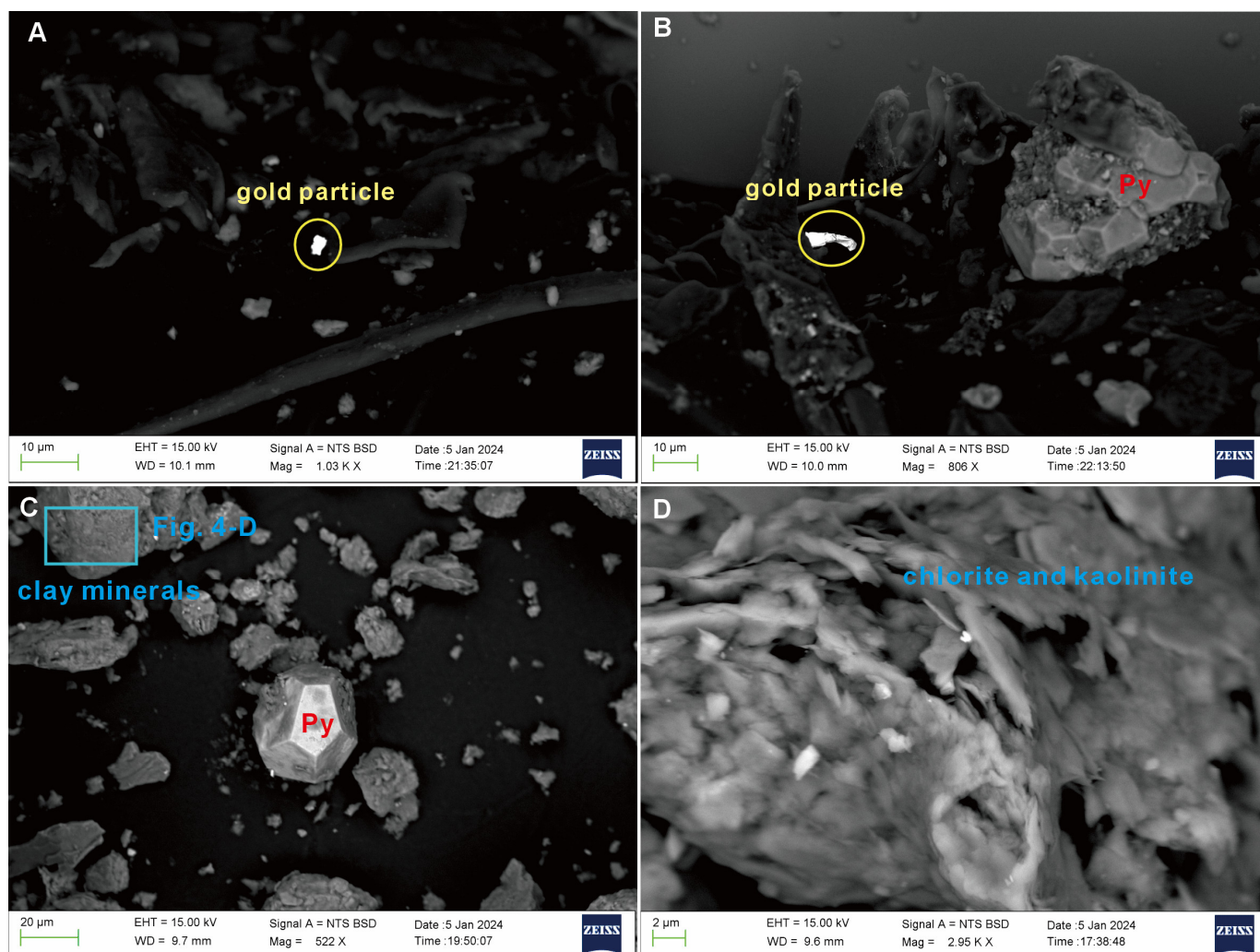


Figure 4. Minerals in altered rock observed by SEM. (A) The micro-native gold particle is marked with a yellow circle. (B) A micro-native gold particle and a group of pyrites. (C) Aggregations of clay minerals and pyrite. (D) The aggregation of chlorite and kaolinite. Py: pyrite.

4.3. TEM Observation of the Altered Rock

Figure 5 shows the particles in altered rocks on a nanoscale. It can be seen that this sample is mainly composed of two minerals; one is irregular and granular, and the other shows a hollow tubular crystal form. The tubular mineral is identified as halloysite based on its chemical composition and size, measuring approximately 700 nm long and 60–70 nm wide, with an outer diameter of 60–70 nm and an inner diameter of 20–30 nm, and a wall thickness of 15–20 nm. There are a large number of gold nanoparticles adsorbed on halloysite, and the particle sizes are generally less than 10 nm (Figure 5A–C). However, we did not find gold nanoparticles adsorbed on the chlorite or kaolinite.

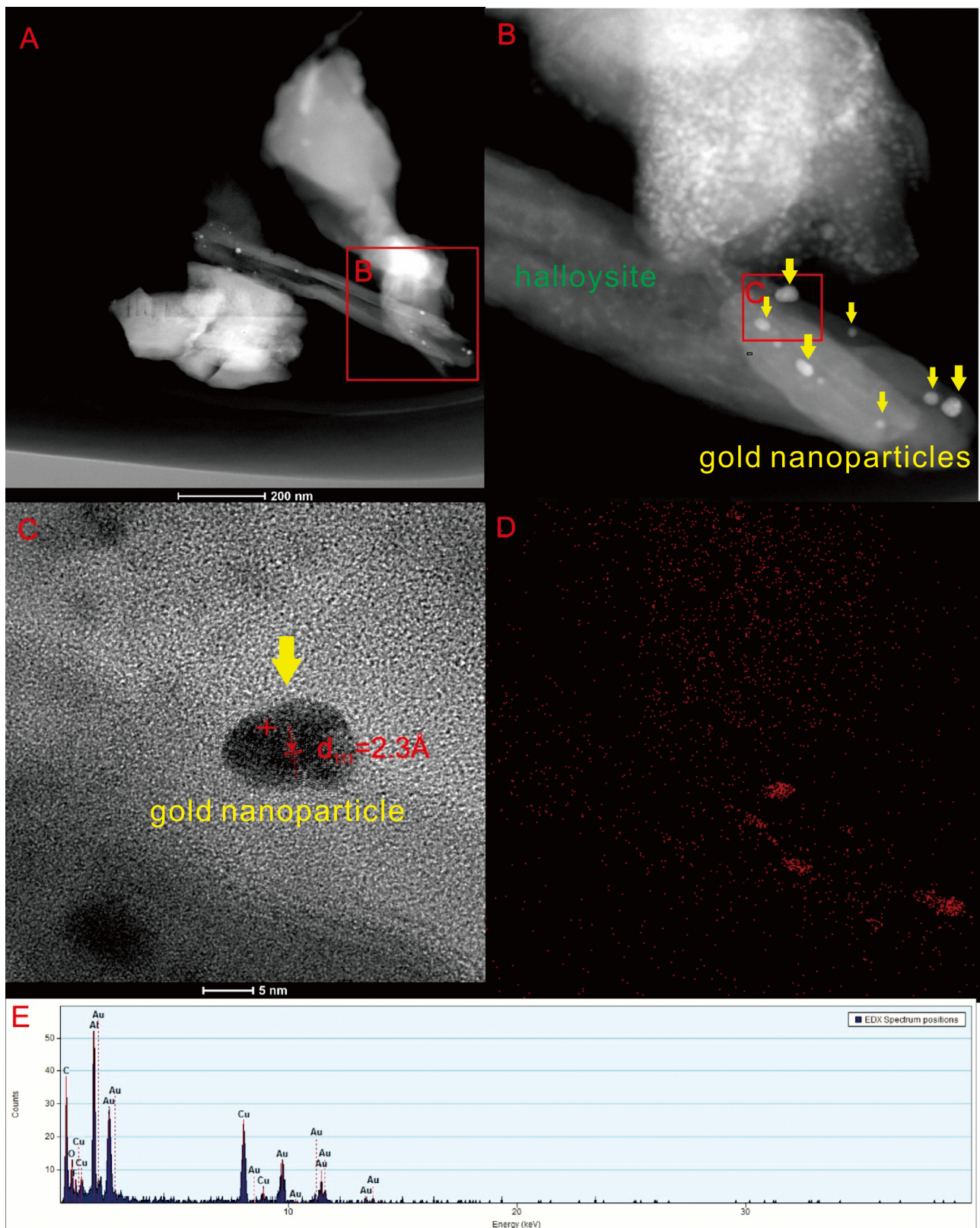


Figure 5. Colloidal gold adsorbed on the halloysite in the altered zone observed with TEM. (A,B) Gold nanoparticles marked by yellow arrows scattered on the surface of halloysite. (C) HRTEM images of nano-gold particles. The measured lattice spacing is 2.3 Å. Electron diffraction patterns indicate that this particle is a polycrystalline aggregate. (D) Surface scanning of (B). The red pixel points represent Au. (E) The EDS spectrum of the gold nanoparticle shown in (C).

5. Discussion

5.1. Gold May Migrate as Colloidal Gold in the Ore-Forming Fluid of Orogenic Gold Deposits

Gold nanoparticles have been reported in various geological environments in recent years, including hot springs, volcanic gas, and hydrothermal fluids in black smokers [17,18,22,29]. Moreover, gold nanoparticles have been detected in CO₂-rich gas-liquid inclusions in the gold-rich layer (9500–11,000 m) of the Russian Kola Super-Deep Borehole [28], providing direct evidence that colloidal gold can still be produced and stably exist under high temperature and pressure conditions. However, there is still a lack of understanding of why colloidal gold can exist in a high-temperature and high-pressure environment.

Colloidal silica may act as a protective agent for colloidal gold. In a simulation experiment, gold colloids can exist stably at a temperature of 350 °C with colloidal silica [15]. Colloidal silica is negatively charged when the pH is higher than ~4, which can enhance the repulsive force of colloidal gold, thereby promoting its stability [49,50]. Synchrotron X-ray Near-edge Spectroscopy (XANES) was used to study the stability of colloidal gold in solutions containing sulfur and citrate [50]. It was found that gold nanoparticles in sulfur-bearing systems begin to lose stability when heated to 150 °C under a pressure of 28 bar. However, after adding 0.5–1.5 wt% colloidal silica, the colloidal gold can remain stable up to 300 °C. When the temperature rises to 350 °C, colloidal gold will precipitate due to the instability of colloidal silica. This result is consistent with the experimental findings of Frondel [15], and it is the first to prove that colloidal gold can exist stably at high temperatures (up to 300 °C) in a sulfur-bearing fluid. In most gold deposits, gold dendrites are commonly hosted by quartz, which implies the co-migration and co-precipitation of colloidal gold and colloidal silica [12,14,51–53].

Dynamic light scattering (DLS) technique combined with a flow type high temperature and high-pressure sample cell (25 °C–375 °C, 250 bar) was used to study the dispersion stability of colloids in supercritical water, and the result showed that the aggregation of colloids in supercritical water was a universal phenomenon irrespective of the materials [54]. The reason is that under the conditions of high temperature and high pressure, the dielectric constant of water decreases, and the electrostatic repulsive potential between particles in the stable dispersion is significantly reduced, causing the agglomeration and sedimentation of colloids. However, this study did not consider the effects of other electrolytes present in geological fluids [54]. Compared to pure water, geological fluids contain abundant substances such as various anions, cations, ion groups, carbon dioxide, methane, etc., which play a vital role in the mineralization process [55]. The electrolyte content in geological fluids can be quantified by salinity [56]. Increasing salinity is often thought to increase the ionic strength of the aqueous medium, thereby stabilizing electrostatic repulsion and leading to the agglomeration and sedimentation of colloids [15,57,58]. The stability of the gold sol to the electrolyte sodium chloride increased with an increase in temperature, indicating an interaction between the factors that affect the stability of the colloid [15]. As temperature increases, the colloid can exist stably at higher salinities. The classic DLVO (Derjaguin–Landau–Verwey–Overbeek) theory was used to calculate the inter-particle forces at higher temperatures and pressures (500 bar < P < 3000 bar, 25 °C < T < 400 °C) and evaluate the stability of gold colloids and silica colloids in a dilute sodium chloride solution [57]. The results showed that increasing temperature reduces the stability of the colloids. On the contrary, increasing pressure makes the colloids more stable. When the pressure is increased to a certain level (P > 1 kbar), the influence of temperature on the stability of the colloid will be diminished [57].

Besides high pressure and low salinity, the ubiquitous CO₂ in orogenic gold mineralizing fluids may enhance the stability of colloidal gold. Although the high CO₂ content in ore-forming fluids is closely related to orogenic gold deposits [34,59] and has been widely recognized [60,61], the role of CO₂ in gold transport and deposition remains unappreciated [27]. Numerous studies have proved that CO₂-rich fluids have a strong ability to transport gold under high temperature and high pressure conditions, such as low-salinity

CO₂-rich inclusions with a gold content of up to 5 µg/g discovered from the Sigma gold deposit in Vald'Or, Canada [59] and an average gold nanoparticle content of up to 750 µg/g in the CO₂-rich gas-liquid inclusions detected in the gold-rich layer of the Russian Kola Super-deep Borehole [28]. While traditional knowledge suggests that gold is mainly transported in the form of complexes in aqueous fluids, it cannot be ignored that these gold complexes have relatively low predicted solubility in typical gold mine fluids [62,63]. It is difficult to form some spatially discontinuous ultra-high-grade gold veins [30].

Regarding the role of CO₂ in gold transportation, Phillips and Evans [60] proposed that CO₂ dissociates as a weak acid in the ore-forming fluid and acts as a buffer to keep the fluid pH at a proper range. Under this appropriate pH level, it is beneficial to the complexation of HS⁻ and gold, which promotes the maintenance of the gold concentration in the fluid at a higher level [60,64]. However, this explanation was proven to be incorrect [9]. CO₂ may form bicarbonate (HCO₃⁻) and carbonate (CO₃²⁻) ions as ligands for some "hard" metals (such as REE, Ca, Sr, Sn, Zr, U, Nb, etc.), but these two ligands have a low affinity for gold. Moreover, the abundance of HCO₃⁻ and CO₃⁻ ions in the high temperature and high pressure environment of the magma hydrothermal system is very low [6,65,66].

Another well-known function of CO₂ is to enlarge the pressure range of vapor-liquid immiscibility, which causes vapor-liquid separation to occur at a deeper depth. The effect on gold transportation is that it can make the gold fractionate into the gas phase earlier when it is transported upward from the deep [67–69]. Nevertheless, existing data indicate that gold tends to enter the vapor phase during vapor-liquid separation in magmatic hydrothermal conditions. The distribution coefficient ($K_{\text{vap/liq}}$) of gold in the vapor and liquid phases is generally above 1 and can even reach up to ~100, with absolute concentrations of gold in the vapor phase attaining values of 10 µg/g ([6,70] and references therein).

Additionally, CO₂ is nonpolar, and an increase in CO₂ content in the system can lead to a decrease in water activity and fluid dielectric constant, thereby reducing the concentration of solute in the system [68,71]. Kokh et al. [72] explored the effect of CO₂ on the dissolution of gold under hydrothermal conditions and obtained direct experimental data on the solubility of gold in supercritical CO₂-H₂O-S-salt fluid for the first time. Under the conditions of 450 °C, 2 kbar, and 7 wt% (NaCl + KCl), the solubility of gold in neutral sulfur-poor fluids (0.1 wt% S) remains stable at around 0.1 µg/g with the increase in CO₂ content, while the solubility of gold in acidic sulfur-rich fluids (1 wt% S) decreases from 2 µg/g at 0 wt% CO₂ to 0.2 µg/g at 70 wt% CO₂. It was explained that gold in sulfur-poor fluids mainly forms a neutral complex (AuHS)₀, while gold in sulfur-rich fluids is mainly transported in the form of Au(HS)₂⁻, which becomes less stable with the increase in CO₂ content [72]. This work helps us to understand the effect of CO₂ on the transport of gold under supercritical conditions.

However, the solubility of gold complexes is obviously lower than the gold concentration detected in some natural CO₂-rich inclusions [28]. Therefore, it is reasonable to assume that large amounts of gold may exist as colloid in CO₂-rich fluids. In nanomaterials science, a method has been developed for preparing gold nanoparticles using organometallic compounds in a supercritical CO₂-water emulsion. This method highlights that gold nanoparticles can be stable in CO₂ fluid, and the high dispersion stability of nanoparticles is attributed to the combination of organic ligands on the surface of nanoparticles [73–75]. The experimental results of Liu et al. [50] also supported this point. The gold colloids in the citrate-based solutions agglomerate and precipitate at 260 °C, which coincides with the instability temperature of citrate (<260 °C). It was speculated that the presence of organic ligands in the fluid could help stabilize the gold colloid.

The early ore-forming fluid of Shangong gold deposits generally has the following characteristics: salinity is generally less than 9%, and the phase proportion of CO₂ ranges from 20% to 70%, matching well with the orogenic gold deposits [34]. Moreover, the pressure of the early mineralization period of the Shangong gold deposit is near 1 kbar (0.93 kbar) [33]. These conditions make it feasible that colloidal gold can exist stably in the early ore-forming fluid.

5.2. Precipitation and Occurrence of Gold in the Alteration Zone

The ore-forming hydrothermal fluid will undergo an alteration reaction to form the alteration zone when encountering suitable wall rocks during the upwelling process, and at least a part of the gold will be unloaded and precipitated from the hydrothermal fluid [34]. Clay minerals, including chlorite, illite, and kaolinite, are widely present in the structural alteration zone of orogenic gold deposits [76,77]. In this study, two types of gold particles were observed in the alteration zone, namely nanoscale native gold particles adsorbed on halloysite (Figure 5B) and unbounded microscale native gold particles (Figure 4A,B).

Clay minerals have a high adsorption capacity for many elements [78,79]. Some scholars have studied and reported on the adsorption of different forms of gold by clay minerals [80]. In the Shewushan supergene gold deposit in China, it was found that gold particles are adsorbed on the edges of clay minerals (such as kaolinite and illite) and goethite, and most of the particles are less than 20 nm [81]. In the Hardrock Archean orogenic gold deposits, part of the gold is found to be adsorbed on chlorite in the orogenic gold ore [82]. The positive correlation between gold and loss on ignition (LOI) in drill core samples from the orogenic gold deposit further verified the fact that part of the gold may be present in clay minerals [83]. However, gold nanoparticles are just found bound to halloysite in this paper, which may be attributed to the tubular shape of hallosite. None are adsorbed on more common clay minerals, such as chlorite and kaolinite, in the alteration zone. The gold nanoparticles on halloysite may be formed by the direct precipitation of colloidal gold from the parent hydrothermal fluid [84–86]. Meanwhile, the microscale native gold particles may originate from the growth of nanoscale gold particles by Ostwald ripening.

6. Conclusions

We observed nano-scale gold particles adsorbed on the halloysite in the altered rock from the Shanggong gold deposit. Based on previous research, we discussed the possibility of gold migration in the form of colloidal gold in the ore-forming fluid of orogenic gold deposits. Increasing temperature and salinity can promote the instability and agglomeration of gold colloid, while increasing pressure is conducive to the stability of colloidal gold. Especially under higher pressure conditions (>1 kbar), the negative effect of temperature on the stability of colloidal gold can be hampered. Silica colloid can protect the gold colloid below 350 °C and maintain its stability in the fluid. Besides complexing with gold ions, various ligands in the fluid may have a positive effect on the stability of colloidal gold. The effect of CO₂ is currently unclear, but it may play an important role in the formation of gold aerosols. Low salinity and an appropriate amount of CO₂ are conducive to the stability of colloidal gold. Orogenic gold deposits usually form at a depth of 2–20 km and under pressure above 1 kbar. Under these geological conditions, the negative effects of high temperatures (higher than 300 °C) on the stability of colloidal gold will be overwhelmed by the positive effects of high pressure. Therefore, during the formation of orogenic gold deposits, it is possible for gold to migrate in the form of colloids.

We propose a viable model to explain the origin of the gold particles in the alteration zone. The gold and fluid of the Shanggong gold deposit may have originated from the metasomatized mantle and Taihua complex. Under high temperature and high pressure, the fluid enters a supercritical state, carrying a large amount of colloidal gold and gold complexes. As the fluid rises, the temperature and pressure decrease, and the supercritical state is left behind. Part of the collaurum is adsorbed by the clay minerals produced by hydrothermal alteration. The other part of the collaurum undergoes growth and evolves into micro-submicrometer-sized gold particles.

Our work is a preliminary analysis of the role of colloidal gold in orogenic gold deposits. More investigations are needed to confirm it, such as detecting gold nanoparticles in fluid inclusions with SP-LA-ICP-MS, distinguishing collaurum from micro-scale gold particles in pyrites and quartz with FIB-SEM and TEM.

Author Contributions: Conceptualization, Z.H.; methodology, Y.Q. and H.L.; validation, B.Z.; investigation, Y.Q., Z.H., X.W. and C.D.; resources, B.Z.; data curation, Y.Q., Z.H. and X.W.; writing—original draft, Y.Q. and Z.H.; writing—review and editing, Z.H. and H.L.; visualization, C.D.; supervision, B.Z.; funding acquisition, Z.H. and H.L. All authors have read and agreed to the published version of the manuscript.

Funding: This research was funded by National Nonprofit Institute Research Grant of CAGS [JKYZD202327], Guangxi Natural Science Foundation [GuikeAD23026129] and National Key Research and Development Program of China [2016YFC0600600].

Data Availability Statement: Data that support the findings of this study are available from the corresponding author upon reasonable request.

Acknowledgments: Thanks are given to two anonymous reviewers for their constructive comments and suggestions. The academic editor helps a lot in the format of this manuscript. Yaowen Liu and Sukun Zhang provided the necessary help for field work. Mei Lu conducted the TEM observation.

Conflicts of Interest: Yu Qiao was employed by the Zijin Mining Group Co., Ltd. The remaining authors declare that the research was conducted in the absence of any commercial or financial relationships that could be construed as a potential conflict of interest.

References

1. Zhai, M.G.; Wu, F.Y.; Hu, R.Z.; Jiang, S.Y.; Li, W.C.; Wang, R.C.; Wang, D.H.; Qi, T.; Qin, K.Z.; Wen, H.J. Critical metal mineral resources: Current research status and scientific issues. *Bull. Natl. Nat. Sci. Found. China* **2019**, *33*, 106–111, (In Chinese with English Abstract)
2. Liu, W.; Etschmann, B.; Testemale, D.; Hazemann, J.; Rempel, K.; Müller, H.; Brugger, J. Gold transport in hydrothermal fluids: Competition among the Cl, Br, HS and NH₃(aq) ligands. *Chem. Geol.* **2014**, *376*, 11–19. [[CrossRef](#)]
3. Pokrovski, G.S.; Tagirov, B.R.; Schott, J.; Bazarkina, E.F.; Hazemann, J.L.; Proux, O. An in situ X-ray absorption spectroscopy study of gold-chloride complexing in hydrothermal fluids. *Chem. Geol.* **2009**, *259*, 17–29. [[CrossRef](#)]
4. Seward, T.M. Thio complexes of gold and the transport of gold in hydrothermal ore solutions. *Geochim. Cosmochim. Acta* **1973**, *37*, 379–399. [[CrossRef](#)]
5. Zezin, Y.D.; Migdisov, A.A.; Williams-Jones, A.E. The solubility of gold in H₂O–H₂S vapor at elevated temperature and pressure. *Geochim. Cosmochim. Acta* **2011**, *75*, 5140–5153. [[CrossRef](#)]
6. Pokrovski, G.S.; Akiniev, N.N.; Borisova, A.Y.; Zotoz, A.V.; Kouzmanov, K. Gold speciation and transport in geological fluids: Insights from experiments and physical-chemical modelling. *Geol. Soc. Lond. Spec. Publ.* **2014**, *402*, 9–70. [[CrossRef](#)]
7. Pokrovski, G.S.; Dubessy, J. Stability and abundance of the trisulfur radical ion S³⁻ in hydrothermal fluids. *Earth Planet. Sci. Lett.* **2015**, *411*, 298–309. [[CrossRef](#)]
8. Pokrovski, G.S.; Dubrovinsky, L.S. The S³⁻ Ion Is Stable in Geological Fluids at Elevated Temperatures and Pressures. *Science* **2011**, *311*, 1052–1054. [[CrossRef](#)]
9. Pokrovski, G.S.; Kokh, M.A.; Guillaume, D.; Borisova, A.Y.; Gisquet, P.; Hazemann, J.-L.; Lahera, E.; Del Net, W.; Proux, O.; Testemale, D.; et al. Sulfur radical species form gold deposits on earth. *Proc. Natl. Acad. Sci. USA* **2015**, *112*, 13484. [[CrossRef](#)]
10. Barré, G.; Truche, L.; Bazarkina, E.F.; Michels, R.; Dubessy, J. First evidence of the trisulfur radical ion S₃⁻ and other sulfur polymers in natural fluid inclusions. *Chem. Geol.* **2017**, *462*, 1–14. [[CrossRef](#)]
11. Gopon, P.; Douglas, J.O.; Auger, M.A.; Hansen, L.; Wade, J.; Cline, J.S.; Robb, L.J.; Moody, M.P. A Nanoscale Investigation of Carlin-Type Gold Deposits: An Atom-Scale Elemental and Isotopic Perspective. *Econ. Geol.* **2019**, *114*, 1123–1133. [[CrossRef](#)]
12. Saunders, J.A. Colloidal transport of gold and silica in epithermal precious-metal systems: Evidence from the Sleeper deposit, Nevada. *Geology* **1990**, *18*, 757–760. [[CrossRef](#)]
13. Saunders, J.A.; Schoenly, P.A. Boiling, colloid nucleation and aggregation, and the genesis of bonanza Au-Ag ores of the sleeper deposit, Nevada. *Miner. Depos.* **1995**, *30*, 199–210. [[CrossRef](#)]
14. Herrington, R.J.; Wilkinson, J.J. Colloidal gold and silica in mesothermal vein systems. *Geology* **1993**, *21*, 539–542. [[CrossRef](#)]
15. Frondel, C. Stability of colloidal gold under hydrothermal conditions. *Econ. Geol.* **1938**, *33*, 1–20. [[CrossRef](#)]
16. Hough, R.M.; Noble, R.; Reich, M. Natural gold nanoparticles. *Ore Geol. Rev.* **2011**, *42*, 55–61. [[CrossRef](#)]
17. Hannington, M.; Hareardóttir, V.; Garbe-Schönberg, D.; Brown, K.L. Gold enrichment in active geothermal systems by accumulating colloidal suspensions. *Nat. Geosci.* **2016**, *9*, 299–302. [[CrossRef](#)]
18. Taran, Y.A.; Bernard, A.; Gavilanes, J.C.; Africano, F. Native gold in mineral precipitates from high temperature volcanic gases of Colima volcano, Mexico. *Appl. Geochem.* **2000**, *15*, 337–346. [[CrossRef](#)]
19. Larocque, A.; Stimac, J.A.; Siebe, C.; Greengrass, K.; Chapman, R.; Mejia, S.R. Deposition of a high-sulfidation Au assemblage from a magmatic volatile phase, Volcán Popocatepetl, Mexico. *J. Volcanol. Geoth. Res.* **2008**, *170*, 51–60. [[CrossRef](#)]
20. Wang, X.Q.; Dong, B.M.; Lin, X.; Xu, S.F.; Yao, W.S.; Ye, R. Geochemical challenges of diverse regolith-covered terrains for mineral exploration in China. *Ore Geol. Rev.* **2016**, *73*, 417–431.

21. Hannington, M.; Garbe-Schnberg, D. Detection of Gold Nanoparticles in Hydrothermal Fluids. *Econ. Geol.* **2019**, *114*, 397–400. [[CrossRef](#)]
22. Gartman, A.; Hannington, M.; Jamieson, J.W.; Peterkin, B.; Garbe-Schönberg, D.; Findlay, A.J.; Fuchs, S.; Kwasnitschka, T. Boiling-induced formation of colloidal gold in black smoker hydrothermal fluids. *Geology* **2018**, *46*, 39–42. [[CrossRef](#)]
23. Reith, F.; Cornelis, G. Effect of soil properties on gold- and platinum nanoparticle mobility. *Chem. Geol.* **2017**, *466*, 446–453. [[CrossRef](#)]
24. Groves, D.I.; Goldfarb, R.J.; Robert, F.; Hart, C.J. Gold Deposits in Metamorphic Belts: Overview of Current Understanding, Outstanding Problems, Future Research, and Exploration Significance. *Econ. Geol.* **2003**, *98*, 1–29.
25. Hou, Z.; Wang, Q.; Zhang, H.; Xu, B.; Yu, N.; Wang, R.; Groves, I.D.; Zheng, Y.; Han, S.; Gao, L.; et al. Lithosphere architecture characterized by crust–mantle decoupling controls the formation of orogenic gold deposits. *Natl. Sci. Rev.* **2023**, *10*, nwac257. [[CrossRef](#)] [[PubMed](#)]
26. Klein, E.L.; Fuzikawa, K. Origin of the CO₂-only fluid inclusions in the Palaeoproterozoic Carará vein-quartz gold deposit, Ipitinga Auriferous District, SE-Guiana Shield, Brazil: Implications for orogenic gold mineralisation. *Ore Geol. Rev.* **2010**, *37*, 31–40. [[CrossRef](#)]
27. Gorczyk, W.; Gonzalez, C.M.; Hobbs, B. Carbon dioxide as a proxy for orogenic gold source. *Ore Geol. Rev.* **2020**, *127*, 103829. [[CrossRef](#)]
28. Prokofiev, V.Y.; Banks, D.A.; Lobanov, K.V.; Selektor, S.L.; Milichko, V.A.; Akinfiyev, N.N.; Borovikov, A.A.; Lüders, V.; Chicherov, M.V. Exceptional Concentrations of Gold Nanoparticles in 1,7 Ga Fluid Inclusions from the Kola Superdeep Borehole, Northwest Russia. *Sci. Rep.* **2020**, *10*, 1108. [[CrossRef](#)]
29. Banks, D.A.; Bozkaya, G.; Bozkaya, O. Direct observation and measurement of Au and Ag in epithermal mineralizing fluid. *Ore Geol. Rev.* **2019**, *111*, 102955. [[CrossRef](#)]
30. Mcleish, D.F.; Williams-Jones, A.E.; Vasyukova, O.V.; Clark, J.R.; Board, W.S. Colloidal transport and flocculation are the cause of the hyperenrichment of gold in nature. *Proc. Natl. Acad. Sci. USA* **2021**, *118*, e2100689118. [[CrossRef](#)]
31. Chen, Y.J.; Pirajno, F.; Qi, J.P. The Shangong gold deposit, Eastern Qinling Orogen, China: Isotope geochemistry and implications for ore genesis. *J. Asian Earth. Sci.* **2008**, *33*, 52–266. [[CrossRef](#)]
32. Fan, H.R.; Xie, Y.H.; Wang, Y.L. Fluid-Rock Interaction during Mineralization of the Shangong Structure-Controlled Alteration-Type Gold Deposit in Western Henan Province, Central China. *Acta. Petrol. Sin.* **1998**, *14*, 529–541, (In Chinese with English Abstract)
33. Wang, J.D.; Ren, Y.Z.; Du, X.Y.; Xia, W.Z.; Yue, H.; Sun, C.Y.; Sun, L.F. Characteristics of ore-forming fluids of Shangong gold deposit in western Henan. *Gold* **2022**, *43*, 19–25, (In Chinese with English Abstract)
34. Goldfarb, R.J.; Groves, D.I. Orogenic gold: Common or evolving fluid and metal sources through time. *Lithos* **2015**, *233*, 2–26. [[CrossRef](#)]
35. Li, R.; Wang, X.; Yang, L.; Zhang, B.; Liu, Q.; Liu, D. The characteristic of microstructural deformation of gold bearing pyrite in Jiaodong: The links between nanoscale gold enrichment and crystal distortion. *Ore Geol. Rev.* **2020**, *122*, 103495. [[CrossRef](#)]
36. Han, Z.; Zhang, B.; Wu, H.; Liu, H.; Qiao, Y.; Zhang, S. Microscopic characterization of metallic nanoparticles in ore rocks, fault gouge and geogas from the Shangong gold deposit, China. *J. Geochem. Explor.* **2020**, *217*, 106562. [[CrossRef](#)]
37. Chen, Y.J.; Franco, P.; Qi, J.P.; Li, J.; Wang, H.H. Ore geology, fluid geochemistry and genesis of the Shangong gold deposit, eastern Qinling Orogen, China. *Resour. Geol.* **2006**, *56*, 99–116. [[CrossRef](#)]
38. Meng, L.; Lan, C.; Zhan, Q.; Wu, Q.; Zhao, T. Origin of the Shangong gold deposit, the southern margin of the North China Craton: Constraints from Rb-Sr ages of sericite, and trace elements and sulfur isotope of pyrite. *Ore Geol. Rev.* **2022**, *142*, 104728. [[CrossRef](#)]
39. Hu, X.L.; He, M.C.; Yao, S.Z. New understanding of the source of ore-forming material and fluid in the Shangong gold deposit, east Qinling. *Acta. Geol. Sin.* **2013**, *87*, 91–100, (In Chinese with English Abstract)
40. Li, J.W.; Bi, S.J.; Selby, D.; Chen, L.; Vasconcelos, P.; Thiede, D.; Zhou, M.F.; Zhao, X.F.; Li, Z.K.; Qiu, H.N. Giant Mesozoic gold provinces related to the destruction of the North China Craton. *Earth Planet. Sci. Lett.* **2012**, *349–350*, 26–37. [[CrossRef](#)]
41. Tang, K.F. *Characteristics, Genesis, and Geodynamic Setting of Representative Gold Deposits in the Xiong’ershan District, Southern Margin of the North China Craton*; China University of Geosciences: Wuhan, China, 2014. (In Chinese)
42. Ren, Z.Y.; Li, J.W. Mineralization characteristics and metallogenic age of Shangong gold deposit in western Henan Province. *Miner. Depos.* **2010**, *29*, 987–988. (In Chinese)
43. Mao, J.W.; Xie, G.Q.; Zhang, Z.H.; Li, X.F.; Wang, Y.T.; Zhang, C.Q.; Li, Y.F. Mesozoic large-scale metallogenic pulses in North China and corresponding geodynamic settings. *Acta Petrol. Sin.* **2005**, *21*, 171–190, (In Chinese with English Abstract)
44. Wu, F.Y.; Lin, J.Q.; Wilde, S.A.; Yang, J.H. Nature and significance of the Early Cretaceous giant igneous event in eastern China. *Earth Planet. Sci. Lett.* **2005**, *233*, 103–119. [[CrossRef](#)]
45. Zhang, D.T.; Feng, J.Z.; Li, L.; Meng, X.F.; He, J.; Liu, Z.Y.; Xu, W.C. Discussion on Post-collision Lithospheric Evolution and Au-Mo Mineralization in the Southern Margin of the North China Craton. *Geotecton. Metallog.* **2015**, *39*, 300–314, (In Chinese with English Abstract)
46. Wang, C.M.; Deng, J.; Zhang, S.T. Relationship between Huashan granite and gold mineralization in Xiong’ershan area, Henan. *Geoscience* **2006**, *20*, 315–321, (In Chinese with English Abstract)

47. Chen, Y.J.; Zhai, M.G.; Jiang, S.Y. Significant achievements and open issues in study of orogenesis and metallogenesis surrounding the North China continent. *Acta Petrol. Sin.* **2009**, *25*, 2695–2726, (In Chinese with English Abstract)
48. Zhang, S.K.; Shi, B.T.; Wang, J.H.; Deng, H.L.; Tian, H.T.; Yan, Z.X.; Feng, S.P.; Zhang, H. Characteristics of isotopic compositions and metallogenic model of Jijiawa gold deposit in the western Henan. *Miner. Explor.* **2016**, *7*, 552–560, (In Chinese with English Abstract)
49. Kobayashi, M.; Juillerat, F.; Galletto, P.; Bowen, P.; Borkovec, M. Aggregation and Charging of Colloidal Silica Particles: Effect of Particle Size. *Langmuir* **2005**, *21*, 5761–5769. [[CrossRef](#)]
50. Liu, W.; Chen, M.; Yang, Y.; Mei, Y.; Etschmann, B.; Brugger, J.; Johannessen, B. Colloidal gold in sulphur and citrate-bearing hydrothermal fluids: An experimental study. *Ore Geol. Rev.* **2019**, *114*, 103142. [[CrossRef](#)]
51. Saunders, J.A. Silica and gold textures in bonanza ores of the Sleeper Deposit, Humboldt County, Nevada: Evidence for colloids and implications for epithermal ore-forming processes. *Econ. Geol.* **1994**, *89*, 628–638. [[CrossRef](#)]
52. Saunders, J.A.; Burke, M.; Brueseke, M.E. Scanning-electron-microscope imaging of gold (electrum) nanoparticles in middle Miocene bonanza epithermal ores from northern Nevada, USA. *Miner. Depos.* **2020**, *55*, 389–398. [[CrossRef](#)]
53. Saunders, J.A.; Burke, M. Formation and aggregation of gold (electrum) nanoparticles in epithermal ores. *Minerals* **2017**, *7*, 163. [[CrossRef](#)]
54. Ghosh, S.K.; Alargova, R.G.; Deguchi, S.; Tsujii, K. Dispersion stability of colloids in sub- and supercritical water. *J. Phys. Chem. B* **2006**, *110*, 25901–25907. [[CrossRef](#)]
55. Chen, Y.J.; Ni, P.; Fan, H.R.; Lai, Y.; Su, W.C.; Zhang, H. Diagnostic fluid inclusions of different types hydrothermal gold deposits. *Acta Petrol. Sin.* **2007**, *23*, 2085–2108, (In Chinese with English Abstract)
56. Hanor, J.S. Origin of saline fluids in sedimentary basins. *Geol. Soc. Lond. Spec. Publ.* **1994**, *78*, 151–174. [[CrossRef](#)]
57. Barton, I. The effects of temperature and pressure on the stability of mineral colloids. *Am. J. Sci.* **2019**, *319*, 737–753.
58. Pamies, R.; Cifre, J.G.H.; Espín, V.F.; Collado-González, M.; Baños, F.G.D.; de la Torre, J.G. Aggregation behaviour of gold nanoparticles in saline aqueous media. *J. Nanopart. Res.* **2014**, *16*, 2376. [[CrossRef](#)]
59. Groves, D.I. The crustal continuum model for late-Archaeon lode-gold deposits of the Yilgarn Block, Western Australia. *Miner. Depos.* **1993**, *28*, 366–374. [[CrossRef](#)]
60. Phillips, G.N.; Evans, K.A. Role of CO₂ in the formation of gold deposits. *Nature* **2004**, *429*, 860–863. [[CrossRef](#)]
61. Garofalo, P.S.; Ficker, M.B.; Gunther, D.; Bersani, D.; Lottici, P.P. Physical-chemical properties and metal budget of Au-transporting hydrothermal fluids in orogenic deposits. *Geol. Soc. Lond. Spec. Publ.* **2014**, *402*, 71–102. [[CrossRef](#)]
62. Stefánsson, A.; Seward, T.M. Gold(I) complexing in aqueous sulfide solutions to 500 °C at 500 bar. *Geochim. Cosmochim. Acta* **2004**, *68*, 4121–4143. [[CrossRef](#)]
63. Williams-Jones, A.E.; Bowell, R.J.; Migdisov, A.A. Gold in Solution. *Elements* **2009**, *5*, 281–287. [[CrossRef](#)]
64. Phillips, G.N.; Powell, R. Formation of gold deposits: A metamorphic devolatilization model. *J. Metamorph. Geol.* **2010**, *28*, 689–718. [[CrossRef](#)]
65. Seward, T.M.; Barnes, H.L. Metal transport by hydrothermal ore fluids. In *Geochemistry of Hydrothermal Ore Deposits.*, 3rd ed.; Barnes, H.L., Ed.; Wiley and Sons: New York, NY, USA, 1997; pp. 435–486.
66. Wood, S.A.; Samson, I.M. Solubility of ore minerals and complexation of ore metals in hydrothermal solutions. *Econ. Geol.* **1998**, *10*, 33–80.
67. Barton, P.B.; Chou, I.M. Refinement of the evaluation of the role of CO₂ in modifying estimates of the pressure of epithermal mineralization. *Econ. Geol.* **1993**, *88*, 873–884. [[CrossRef](#)]
68. Bakker, R.J. Package FLUIDS. Part 3: Correlations between equations of state, thermodynamics and fluid inclusions. *Geofluids* **2009**, *9*, 63–74. [[CrossRef](#)]
69. Kokh, M.A.; Lopez, M.; Gisquet, P.; Lanzanova, A.; Candaudap, F.; Besson, P.; Pokrovski, G.S. Combined effect of carbon dioxide and sulfur on vapor-liquid partitioning of metals in hydrothermal systems. *Geochim. Cosmochim. Acta* **2016**, *187*, 311–333. [[CrossRef](#)]
70. Kouzmanov, K.; Pokrovski, G.S. Hydrothermal controls on metal distribution in porphyry Cu(-Au-Mo) systems. *SEG* **2012**, *16*, 573–618.
71. Walthier, J.V.; Schott, J. The dielectric constant approach to speciation and ion pairing at high temperature and pressure. *Nature* **1988**, *332*, 635–638. [[CrossRef](#)]
72. Kokh, M.A.; Akinfiyev, N.N.; Pokrovski, G.S.; Salvi, S.; Guillaume, D. The role of carbon dioxide in the transport and fractionation of metals by geological fluids. *Geochim. Cosmochim. Acta* **2017**, *197*, 433–466. [[CrossRef](#)]
73. Esumi, K.; Sarashina, S.; Yoshimura, T. Synthesis of gold nanoparticles from an organometallic compound in supercritical carbon dioxide. *Langmuir* **2004**, *20*, 5189–5191. [[CrossRef](#)]
74. Ryoo, W.; Dickson, J.L.; Dhanuka, V.V.; Webber, S.E.; Bonnacaze, R.T.; Johnston, K.P. Electrostatic stabilization of colloids in carbon dioxide: Electrophoresis and dielectrophoresis. *Langmuir* **2005**, *21*, 5914–5923. [[CrossRef](#)] [[PubMed](#)]
75. Yao, H.; Wu, B.; Xu, Z.; Yang, Z.; Yang, X. Solvation structure and dynamics for passivated Au nanoparticle in supercritical CO₂: A molecular dynamic simulation. *J. Colloid. Interf. Sci.* **2011**, *353*, 22–29.
76. Wilde, A.R.; Bierlein, F.P.; Pawlitschek, M. Litho geochemistry of orogenic gold deposits in Victoria, SE Australia: A preliminary assessment for undercover exploration. *J. Geochem. Explor.* **2004**, *84*, 35–50. [[CrossRef](#)]

77. Idrus, A.; Kolb, J.; Meyer, F.M. Mineralogy, Litho-geochemistry and Elemental Mass Balance of the Hydrothermal Alteration Associated with the Gold-rich Batu Hijau Porphyry Copper Deposit, Sumbawa Island, Indonesia. *Resour. Geol.* **2010**, *59*, 215–230. [[CrossRef](#)]
78. Pentrák, M.; Czímerová, A.; Madejová, J.; Komadel, P. Changes in layer charge of clay minerals upon acid treatment as obtained from their interactions with methylene blue. *Appl. Clay Sci.* **2012**, *55*, 100–107. [[CrossRef](#)]
79. Uddin, M.K. A review on the adsorption of heavy metals by clay minerals, with special focus on the past decade. *Chem. Eng. J.* **2017**, *308*, 438–462. [[CrossRef](#)]
80. Rakhila, Y.; Elmchaouri, A.; Mestari, A.; Korili, S.; Abouri, M.; Gil, A. Adsorption recovery of Ag(I) and Au(III) from an electronics industry wastewater on a clay mineral composite. *Int. J. Min. Met. Mater.* **2019**, *26*, 673–680. [[CrossRef](#)]
81. Hong, H.; Tie, L. Characteristics of the minerals associated with gold in the Shewushan supergene gold deposit, China. *Clay Clay Miner.* **2005**, *53*, 162–170. [[CrossRef](#)]
82. Nadeau, O.; Harris, J. Remobilization and adsorption of colloidal gold on nano-particulate chlorite at the Hardrock Archean orogenic gold deposits: A new tool for gold exploration. *J. Geochem. Explor.* **2019**, *204*, 181–205. [[CrossRef](#)]
83. Cruz, N.; Peng, Y.; Farrokhpay, S.; Bradshaw, D. Interactions of clay minerals in copper–gold flotation: Part 1—Rheological properties of clay mineral suspensions in the presence of flotation reagents. *Miner. Eng.* **2013**, *50–51*, 30–37. [[CrossRef](#)]
84. Bakken, B.M.; Hochella, M.F.; Marshall, A.F.; Turner, A.M. High-resolution microscopy of gold in unoxidized ore from the Carlin mine, Nevada. *Econ. Geol.* **1989**, *84*, 171–179. [[CrossRef](#)]
85. Morey, A.A.; Tomkins, A.G.; Bierlein, F.P.; Weinberg, R.F.; Davidson, G.J. Bimodal distribution of gold in pyrite and arsenopyrite: Examples from the Archean Boorara and Bardoc shear systems, Yilgarn craton, Western Australia. *Econ. Geol.* **2008**, *103*, 599–614. [[CrossRef](#)]
86. Palenik, C.S.; Utsunomiya, S.; Reich, M.; Kesler, S.E.; Wang, L.; Ewing, R.C. “Invisible” gold revealed: Direct imaging of gold nanoparticles in a Carlin-type deposit. *Am. Miner.* **2004**, *89*, 1359–1366. [[CrossRef](#)]

Disclaimer/Publisher’s Note: The statements, opinions and data contained in all publications are solely those of the individual author(s) and contributor(s) and not of MDPI and/or the editor(s). MDPI and/or the editor(s) disclaim responsibility for any injury to people or property resulting from any ideas, methods, instructions or products referred to in the content.